

1 **MANUSCRIPT TITLE**

2 Telomeric repeat evolution in the phylum Nematoda revealed by high-quality genome  
3 assemblies and subtelomere structures

4

5 **AUTHORS**

6 Jiseon Lim<sup>1,2</sup>, Wonjoo Kim<sup>1,2</sup>, Jun Kim<sup>1,3,4,\*</sup>, Junho Lee<sup>1,2,3,\*</sup>

7 <sup>1</sup> Department of Biological Sciences, Seoul National University, Gwanak-ro 1, Gwanak-gu,  
8 Seoul 08826, Korea

9 <sup>2</sup> Institute of Molecular Biology and Genetics, Seoul National University, Seoul 08826, Korea

10 <sup>3</sup> Research Institute of Basic Sciences, Seoul National University, Seoul 08826, Korea

11 <sup>4</sup> Department of Convergent Bioscience and Informatics, College of Bioscience and  
12 Biotechnology, Chungnam National University, Daehak-ro 99, Daejeon 34134, Republic of  
13 Korea

14 \* Corresponding authors: [elegans@snu.ac.kr](mailto:elegans@snu.ac.kr) and [junkim@cnu.ac.kr](mailto:junkim@cnu.ac.kr)

15

16 A running title: Telomeric repeat evolution in Nematoda

17

## 18 **ABSTRACT**

19 Telomeres are composed of tandem arrays of telomeric-repeat motifs (TRMs) and telomere-  
20 binding proteins (TBPs), which are responsible for ensuring end-protection and end-  
21 replication of chromosomes. TRMs are highly conserved due to the sequence specificity of  
22 TBPs, although significant alterations in TRM have been observed in several taxa, except  
23 Nematoda. We used public whole-genome sequencing datasets to analyze putative TRMs of  
24 100 nematode species and determined that three distinct branches included specific novel  
25 TRMs, suggesting that evolutionary alterations in TRMs occurred in Nematoda. We focused  
26 on one of the three branches, the Panagrolaimidae family, and performed a *de novo*  
27 assembly of four high-quality draft genomes of the canonical (TTAGGC) and novel TRM  
28 (TTAGAC) isolates; the latter genomes revealed densely clustered arrays of the novel TRM.  
29 We then comprehensively analyzed the subtelomeric regions of the genomes to infer how  
30 the novel TRM evolved. We identified DNA damage–repair signatures in subtelomeric  
31 sequences that were representative of consequences of telomere maintenance mechanisms  
32 by alternative lengthening of telomeres. We propose a hypothetical scenario in which  
33 TTAGAC-containing units are clustered in subtelomeric regions and pre-existing TBPs  
34 capable of binding both canonical and novel TRMs aided the evolution of the novel TRM in  
35 the Panagrolaimidae family.

36

## 37 **INTRODUCTION**

38 Since linear chromosomes originated from a circular structure, a specific DNA–protein  
39 complex has evolved to protect the ends of the chromosomes, i.e. the telomere. Telomeres  
40 are typically composed of tandem arrays of telomeric-repeat motifs (TRMs) and telomere-  
41 binding proteins (TBPs) that can bind to the tandem arrays (Zhong et al. 1992). TBP binding  
42 interferes with the accession of other proteins. Hence, proteins that respond to DNA damage  
43 signals cannot bind to the exposed ends of linear chromosomes and the exposed ends are  
44 not recognized as DNA damage sites (Van Steensel et al. 1998; De Lange 2009; Lazzerini-  
45 Denchi and Sfeir 2016). This enables the telomere to maintain chromosome integrity.

46 TRM sequences are typically well conserved because TBPs attach to arrays of TRMs in a  
47 sequence-specific manner. However, dozens of variant TRMs have evolved in many taxa,  
48 including  $\geq 150$  motifs in fungi (Červenák et al. 2021) and  $\geq 7$  motifs in plants (Peska and  
49 Garcia 2020). Furthermore, except Hymenoptera, many arthropod species have unique  
50 telomere structures. For example, most Insecta species have telomere structures composed  
51 of telomere-specific retrotransposons interposed between canonical TRMs, whereas Diptera  
52 species have telomeres that are exclusively composed of retrotransposons and lack TRMs  
53 (Abad et al. 2004; Garavís et al. 2013; Zhou et al. 2022). It is yet to be elucidated how TRMs  
54 have been altered while interacting with TBPs. These diverse TRMs and telomere structures  
55 developed from the co-evolution of a TRM and several TBPs (Shakirov et al. 2009; Steinberg-  
56 Neifach and Lue 2015; Sepsiova et al. 2016; Červenák et al. 2019); however, they may have  
57 also originated from TRM-specific changes regardless of TBP changes if TBPs were capable  
58 of binding to several types of TRMs (Rotková et al. 2004; Fajkus et al. 2005; Kramara et al.  
59 2010; Visacka et al. 2012; Červenák et al. 2019; Tomáška et al. 2019; Červenák et al. 2021).

60 We focused our analysis on subtelomeric regions and the DNA damage–repair signatures  
61 generated during telomere evolution, especially telomere and subtelomere reconstruction by  
62 alternative lengthening of telomeres (ALT) mechanisms (Heaphy et al. 2011; Sobinoff and  
63 Pickett 2017). ALT, which refers to alternative mechanisms that substitute telomerase  
64 function for telomere maintenance at the chromosome ends (Bryan et al. 1995), is crucial in  
65 telomerase mutant eukaryotic cells such as those in yeast, *Caenorhabditis elegans*, mouse,  
66 and human, and can thus be used to model and interpret the evolution of TRM changes  
67 (Lundblad and Blackburn 1993; Bryan et al. 1995; Seo et al. 2015; Kim et al. 2020; Kim et al.  
68 2021a; Kim et al. 2021b). In these ALT models, homology-directed repair (HDR) mechanisms  
69 can add new telomeric components. HDRs exploit the homology between shortened  
70 telomeric sequences and tandem arrays of TRMs in other genomic loci to replicate the  
71 tandem array and adjacent sequences to the shorter end (Lydeard et al. 2007; Roumelioti et  
72 al. 2016; Kramara et al. 2018; Kim et al. 2020). Furthermore, a unique sequence inserted  
73 between TRMs, known as the template for ALT, may be used to repair shorter telomeric  
74 repeats even in wild-type *C. elegans*, resulting in the formation of a new subtelomeric  
75 structure (Kim et al. 2019a). These findings suggest that ALT mechanisms play an essential  
76 role in the evolution of telomeres and the evolutionary route can be reconstructed by  
77 studying ALT activity traces left in subtelomeric sequences.

78 The present study explored TRM evolution in Nematoda using public whole-genome  
79 sequencing (WGS) data obtained from 100 nematode species and our high-quality genome  
80 assemblies. We evaluated the subtelomeric regions of TTAGGC-telomere isolates of  
81 Panagrolaimidae to infer possible evolutionary paths toward TTAGAC telomeres.

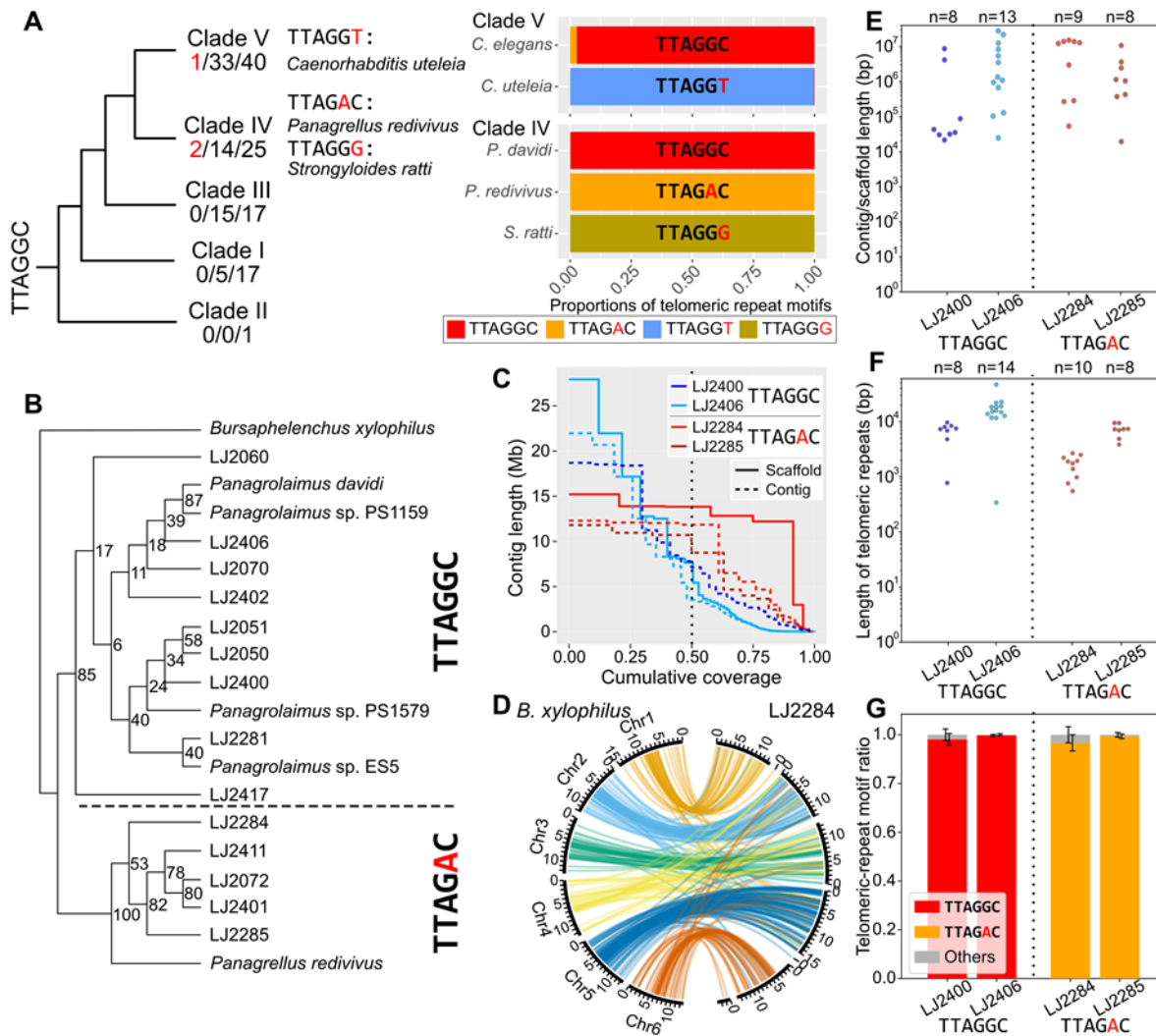
82

## 83 **RESULTS**

### 84 **Identification of three novel TRMs in Nematoda**

85 We examined variations in TRMs using public short-read WGS data from Nematoda species  
86 that have matched public genome assemblies from all five major clades. A total of 100  
87 species met the criteria, including at least 17 species from Clades I, III, IV, and V but only one  
88 from Clade II (Fig. 1A). The species and accession numbers used in this analysis are listed in  
89 Supplemental Table S1 and S2.

90



91

92

93 **Figure 1.** Putative novel TRMs in the phylum Nematoda and validation of the emergence of

94 TTAGAC in the family Panagrolaimidae. (A) The cladogram was adapted and modified from

95 Smythe et al. 2019 (Smythe et al. 2019) with permission from BMC Ecology and Evolution

96 2019, CC BY 4.0 (<https://creativecommons.org/licenses/by/4.0/>). The three numbers

97 separated by '/' under each clade indicates the number of species with novel TRMs/the

98 number of species whose TRM was identified in our analysis/total number of species we

99 analyzed, respectively. Changes from TTAGGC, the canonical Nematoda TRM, to the novel

100 TRMs are highlighted in red. Below each novel TRM is a species name with the  
101 corresponding TRM. Each bar indicates the proportion of the canonical Nematoda TRM  
102 (TTAGGC) and novel TRMs in each species. The upper bar of each pair represents a control  
103 species that harbors the canonical TRM. The TRMs are represented as follows: red, TTAGGC;  
104 orange, TTAGAC; blue, TTAGGT; khaki, TTAGGG. (B) Phylogenetic relationships of 19  
105 Panagrolaimidae species/isolates based on their 18S rDNA sequences and their putative  
106 TRMs. *Bursaphelenchus xylophilus* was used as an outgroup species. The number on each  
107 node represents the bootstrap support value. (C) Contig/scaffold length distributions of the  
108 genome assemblies. The vertical dotted line indicates N50 contig/scaffold size. (D) Synteny  
109 plot of LJ2284 compared to *B. xylophilus*. Each colored line represents a BUSCO gene shared  
110 among the genome assemblies of our four isolates and *B. xylophilus*. Orange lines indicate  
111 that corresponding BUSCO genes are in Chromosome 1 in *B. xylophilus*. Sky blue, bluish  
112 green, yellow, blue, and vermillion represent Chromosomes 2, 3, 4, 5, and 6, respectively. We  
113 used Wong's color palette designed for color-blind individuals (Wong 2011). (E–G) The  
114 vertical dotted line separates the TTAGGC-telomere isolates (left) and the TTAGAC-telomere  
115 isolates (right). (E) Length distributions of the contigs/scaffolds containing highly clustered  
116 telomeric repeats at the end. Each dot represents each contig/scaffold, and the total number  
117 of contigs/scaffolds of each isolate (n) is indicated at the top of the graph. (F) Estimated  
118 length distributions of clustered telomeric repeats at the end of the contigs/scaffolds. Each  
119 dot indicates a telomeric-repeat cluster for each contig/scaffold, and the total number of  
120 telomeric-repeat clusters for each isolate (n) is indicated at the top of the graph. (G) The

121 proportion of TRM types in clustered telomeric repeats. Error bars represent the standard  
122 deviation for all clustered telomeric repeats at the end of contigs/scaffolds in each isolate.

123

124 The canonical TRM of Nematoda is known to be a 6-bp sequence (TTAGGC) that covers  
125 a >1-kb length in *C. elegans* telomeres (Kim et al. 2019a; Yoshimura et al. 2019). We  
126 examined the WGS data from 100 species to identify novel TRMs with a concatemer of 5–7  
127 bp, a high copy number, and a pattern similar to TTAGGC. We determined the TRM in 67  
128 species using the following criterion: TRM repeats should be long concatemers for TBP  
129 binding, so TRM-like *k*-mer counts should be high enough ( $\geq 100$  in 5 million short reads in  
130 our analysis) (Fig. 1A and Supplemental Table S1). However, 26 of the remaining 33 species  
131 exhibited low *k*-mer counts of TRM-like motifs, so we could not determine their TRMs  
132 (Supplemental Table S2). The remaining seven species had high *k*-mer counts, but we  
133 excluded them from the TRM-determined group because of the following reasons: we  
134 detected potential sample or host contamination in *Enoplus brevis*, two *Strongyloides*, and  
135 three *Trichinella* species, and *Diploscapter pachys* had only short concatemers ( $\leq 10$  copies)  
136 in the middle of its reads (Supplemental Table S2; see Supplemental Note for more  
137 information).

138 TTAGGC, the canonical Nematoda TRM, was identified in 64 of the 67 TRM-determined  
139 species (Fig. 1A and Supplemental Table S1). We determined that the other three nematode  
140 species had few TTAGGC copies but a high copy number of one of three putative TRMs:  
141 TTAGGT, TTAGAC, and TTAGGG in *Caenorhabditis uteleia*, *Panagrellus redivivus*, and



142 *Strongyloides ratti*, respectively (Fig. 1A, Supplemental Fig. S1 and Supplemental Tables S1  
143 and S3; see Supplemental Note and Supplemental Table S4 for further validation of the  
144 TRMs). The identified TRMs were new to Nematoda and had not been reported previously.  
145 We assumed that these three motifs evolved independently because they occurred in  
146 phylogenetically distant branches.

#### 147 **The emergence of a new TRM, TTAGAC, in the family Panagrolaimidae**

148 We focused on the TTAGAC sequence of the family Panagrolaimidae to confirm the  
149 noncanonical TRM sequence identified by short-read WGS data because many different  
150 isolates of this family were widely isolated from regions across the Republic of Korea. Some  
151 were easily cultured under laboratory conditions. We used 19 short-read WGS datasets of  
152 the family Panagrolaimidae to determine whether the unique motif TTAGAC emerged once  
153 or multiple times (Supplemental Table S5). WGS datasets of five species were available from  
154 publicly accessible databases, whereas the remainder were derived from sequencing data of  
155 the isolates collected from the Republic of Korea, which were probably distinct species as  
156 they had distinguishable ribosomal DNA (rDNA) sequences (Supplemental Table S6). *B.*  
157 *xylophilus* was also used as the outgroup species.

158 We determined that *Panagrellus redivivus* and five out of fourteen collected isolates had the  
159 novel TRM, TTAGAC, whereas all four *Panagrolaimus* species and the remaining nine isolates  
160 possessed the canonical TRM, TTAGGC. Moreover, the five collected TTAGAC-TRM isolates  
161 clustered with *Panagrellus redivivus*; however, the nine TTAGGC-TRM isolates were grouped  
162 with the *Panagrolaimus* species (Fig. 1B and Supplemental Table S5). Furthermore, the

163 TTAGGC concatemer was not observed in any of the 6 TTAGAC-TRM species/isolates, nor  
164 was the TTAGAC concatemer found in any of the 13 TTAGGC-TRM species/isolates. These  
165 results suggest that TTAGAC sequences in Panagrolaimidae may have arisen from a single  
166 ancestor that had TTAGAC as its TRM.

167 **High-quality genome assemblies confirmed that TTAGAC repeats were clustered at the**  
168 **ends of contigs or pseudo-chromosome molecules in TTAGAC-TRM isolates.**

169 We constructed *de novo* genome assemblies of Panagrolaimidae isolates using PacBio high-  
170 fidelity (HiFi) long-read sequencing technology and Arima Hi-C technology to assess  
171 whether the newly identified TRM presented clusters at the ends of the chromosomes. Two  
172 TTAGAC-TRM isolates, LJ2284 and LJ2285, and two TTAGGC-TRM isolates, LJ2400 and  
173 LJ2406, were selected for the study. We produced 3.1 Gb (43×), 2.9 Gb (55×), 17.4 Gb (26×),  
174 and 36.1 Gb (93×) HiFi reads for LJ2284, LJ2285, LJ2400, and LJ2406, respectively. The HiFi  
175 reads were then assembled into high-quality draft genomes in which the length of the  
176 longest contig and contig N50 varied from 11.80 Mb to 21.96 Mb and 3.28 Mb to 11.84 Mb,  
177 respectively. We also generated Hi-C data for LJ2284 and LJ2406 and scaffolded their contigs  
178 into larger chunks (Supplemental Fig. S2 and Supplemental Table S7). The longest scaffold  
179 lengths increased to 15.2 Mb and 27.9 Mb, and their scaffold N50 increased to 13.8 Mb and  
180 7.6 Mb for LJ2284 and LJ2406, respectively (Fig. 1C and Supplemental Table S8). Additionally,  
181 91.4% of the LJ2284 contigs were connected as five scaffolds (Supplemental Fig. S2).

182 All of our genome assemblies had ~75% BUSCO completeness, which was comparable to  
183 that of the nearly complete genome assembly of *B. xylophilus* (71%) (Supplemental Fig. S3)

184 (Dayi et al. 2020). In addition, we analyzed the synteny relationships between *B. xylophilus*  
185 and our genome assemblies using their common single-copy orthologs. Pseudo-  
186 chromosome-level scaffolds of LJ2284 and contigs of LJ2285 exhibited marked collinearity  
187 for all the chromosomes, except Chromosome 4 of *B. xylophilus* (Fig. 1D, Supplemental Fig.  
188 S4 and Supplemental Note). Chromosomes 5 and 6 of *B. xylophilus* also showed collinearity  
189 with clusters of LJ2400 contigs and LJ2406 scaffolds, but the collinearity of other  
190 chromosomes was much weaker (Supplemental Fig. S4 and Supplemental Note). Based on  
191 these findings, our Panagrolaimidae genome assemblies were highly contiguous.

192 The constructed high-quality genome assemblies revealed that the telomeric repeats of both  
193 LJ2284 and LJ2285 changed from TTAGGC to TTAGAC. First, we confirmed whether the  
194 telomeric repeats had been adequately assembled. Our analysis revealed that each genome  
195 assembly had 8–13 contigs/scaffolds ending with telomeric repeats (Fig. 1E). Among these  
196 contigs/scaffolds, one each of LJ2284 and LJ2406 was assembled at the telomere-to-  
197 telomere level (Supplemental Tables S7 and S8). The telomeric repeats at the ends of the  
198 contigs/scaffolds in each genome assembly exhibited various ranges of length in the  
199 Panagrolaimidae isolates (Fig. 1F and Supplemental Table S9). Their lengths in LJ2284 ranged  
200 from 0.5 to 2.7 kb, but they were much longer in LJ2285 and LJ2400, ranging from 3.8 to 9.7  
201 kb (except for one in LJ2400). LJ2406 exhibited telomeric-repeat clusters longer than 10 kb  
202 (except for one cluster). We identified that 84.9%–99.4% of raw HiFi reads were longer than  
203 10 kb in all four isolates and that LJ2406, which has much longer telomeres than the other  
204 three isolates, had 328 reads consisting only of 10–26-kb telomeric repeats (Supplemental  
205 Fig. S5). Therefore, the TRM cluster lengths at each contig/scaffold end would be highly

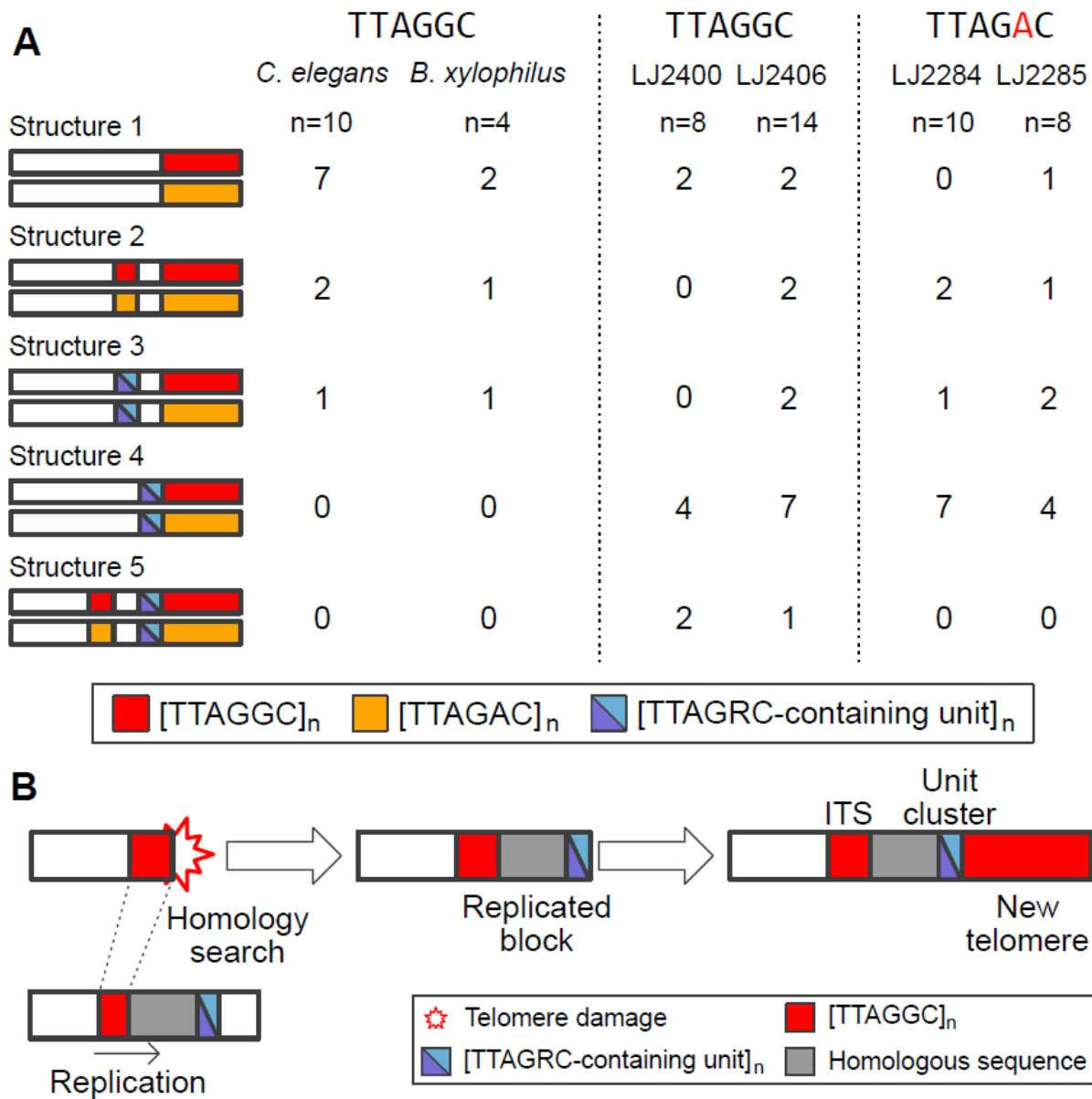
206 correlated with their actual lengths (see Supplemental Note for detailed description). The  
207 lengths of the clustered TRMs were comparable to those of the two *C. elegans* assemblies  
208 constructed using long-read sequencing technologies (2.3–5.7 kb) (Kim et al. 2019a;  
209 Yoshimura et al. 2019). Furthermore, the telomeric repeats consisted mainly of TTAGAC in  
210 LJ2284 (96.67%) and LJ2285 (99.35%) and of TTAGGC in LJ2400 (98.11%) and LJ2406  
211 (99.73%) (Fig. 1G, Supplemental Fig. S6 and Supplemental Table S9). These findings  
212 supported our TRM study employing short-read WGS data and revealed that the TTAGAC  
213 telomere had evolved in the family Panagrolaimidae.

#### 214 **TTAGAC-containing units clustered near telomeric regions of TTAGGC-telomere** 215 **isolates**

216 Because most of the nematode species that we analyzed had a canonical Nematoda TRM  
217 sequence, TTAGGC, the TTAGAC telomere probably evolved from its ancestral TTAGGC  
218 telomere via a single nucleotide mutation of the telomerase RNA component gene. We  
219 hypothesized that subtelomeric sequences can provide evidence regarding the evolutionary  
220 mechanism because these can carry historical records of telomere dynamics. For example, it  
221 has previously been documented that ALT mechanisms have been used to reconstruct  
222 subtelomeric and telomeric regions in *C. elegans* and that templates for ALT in subtelomeric  
223 regions can be used to repair telomere damage or maintain the integrity of the telomere  
224 (Seo et al. 2015; Kim et al. 2019a; Kim et al. 2020; Kim et al. 2021b; Lee et al. 2022b). Thus, we  
225 analyzed subtelomeric regions of our four Panagrolaimidae genome assemblies to trace  
226 ancestral telomere damage and repair events that could explain how the TTAGAC telomere  
227 evolved from the TTAGGC telomere.

228 Most telomeric repeats in telomeric regions (7/10 in LJ2284, 4/8 in LJ2285, 6/8 in LJ2400, and  
229 8/14 in LJ2406) were attached to unit clusters containing TTAGGC or TTAGAC (e.g.  
230 [TTAGGCTTAATTGC]<sub>n</sub> or [TTAGACTTATTCGC]<sub>n</sub>) (Fig. 2A and Supplemental Table S10). This  
231 finding was striking, as none of the subtelomeric regions of *C. elegans* and *B. xylophilus*  
232 exhibited TRM-containing unit clusters directly attached to the telomeric regions (Fig. 2A and  
233 Supplemental Table S11). Furthermore, both TTAGGC-containing unit clusters and TTAGAC-  
234 containing unit clusters were identified in all genomes of the TTAGGC- and TTAGAC-  
235 telomere isolates, with the exception of the LJ2285 genome (TTAGAC telomere), which  
236 contained only TTAGAC-containing unit clusters. For LJ2284, LJ2400, and LJ2406, these  
237 clusters consisted of repetitive units with length distributions ranging from 14 bp to ~2 kb,  
238 and these repetitive units were tandemly repeated on an average of  $\geq 19$  copies  
239 (Supplemental Tables S10 and S12). The LJ2285 genome did not contain such same-length  
240 unit clusters; however, it contained sequence clusters consisting of 5–9 copies of units  
241 containing TTAGAC and similar sequences (10–74 bp). These TRM-containing unit clusters  
242 were not found outside the subtelomeric region in the telomere-containing contigs/scaffolds  
243 (see also Supplemental Note describing a contrasting case in *C. elegans*), raising the  
244 possibility that these clusters are associated with telomere maintenance in Panagrolaimidae.  
245 Notably, we also identified a similar subtelomeric pattern in *Caenorhabditis uteleia*, the  
246 noncanonical TTAGGT-TRM species, where TTAGGT- and/or TTAGGC-containing unit clusters  
247 were attached to or close to long TTAGGT repeat arrays (Supplemental Fig. S7 and  
248 Supplemental Note) (SRA accession: ERR8978452) (The Darwin Tree of Life Project  
249 Consortium 2022).

250



251

252

253 **Figure 2.** Subtelomere structures and a proposed model to explain clustered blocks of TRMs  
 254 or TTAGRC-containing unit clusters in the subtelomeric regions. (A) Schematic representation  
 255 of subtelomere structures in the contigs/scaffolds listed in Supplemental Table S10. We

256 categorized the structure of subtelomeric regions (up to 200 kb from the end of the  
257 telomeric contig/scaffold) using the following criteria: (i) whether it has ITSs (shorter red  
258 blocks) and/or TTAGRC-containing unit clusters (half-sky blue, half-violet blocks) and (ii)  
259 whether ITSs, unit clusters, and telomeric regions were directly attached or separated by  
260 other sequences (white, empty blocks). Each horizontal bar represents a subtelomere  
261 structure with only a telomeric TTAGRC-containing unit cluster (shown in Structure 4 and 5)  
262 and an ITS or a TTAGRC-containing unit cluster closest to the telomere (shown in Structure 2  
263 or 3). Each value refers to the number of contigs/scaffolds with the corresponding structure  
264 type in each species/isolate. TTAGGC-telomere species and isolates had ITSs that were  
265 composed of TTAGGC, rather than TTAGAC, and TTAGAC-telomere species and isolates had  
266 only TTAGAC-type ITSs, too. (B) A proposed model for generating subtelomere structures  
267 responsible for Structure 5. After telomere damage, HDR mechanisms can exploit homology  
268 between shortened telomeric repeats and ITSs at other loci to repair the damaged telomere.  
269 A HDR mechanism, break-induced replication (BIR), may replicate sequences near the ITS,  
270 creating a new homologous block of the original sequence block. If the original template  
271 block exhibits a TTAGRC-containing unit cluster, the cluster would also be replicated. Finally,  
272 a new telomere composed of TTAGGC repeats can be replenished by active telomerase.

273

274 In addition to the TRM-containing unit clusters, interstitial telomeric sequences (ITSs) were  
275 frequently observed in the subtelomeric regions of the constructed genome assemblies,  
276 which were consistent with the ITS enrichment present in *C. elegans* chromosome arms (The  
277 *C. elegans* Sequencing Consortium 1998). All subtelomere structures were categorized based

278 on the location of the unit clusters and/or the ITSs in subtelomeric regions (up to 200 kb  
279 from the end of the telomeric contig/scaffold) (Supplemental Tables S10 and S11). We  
280 annotated a total of 12 subtypes (Supplemental Fig. S8), but for simplicity we merged them  
281 into five major subtelomere structures by considering only telomeric TTAGRC-containing unit  
282 clusters and ITSs or TTAGRC-containing unit clusters closest to the telomere (Structure 1–5 in  
283 Fig. 2A; see Supplemental Fig. S9 for examples of Structure 2–5). Notably, the motif in all ITSs  
284 was the same as their TRM. The four genome assemblies exhibited similar patterns. For most  
285 of the subtelomere structures in the four genome assemblies, the TRM-containing unit  
286 cluster was positioned directly adjacent to the telomeric region. Structure 1, which did not  
287 contain any unit cluster or ITS, accounted for fewer than a quarter of all the subtelomere  
288 structures (the lengths of telomeres in Structure 1 differ from those of ITSs in *C. elegans* and  
289 our four isolates; see Supplemental Note). In contrast, Structure 2–5 had at least one unit  
290 cluster or ITS separated from the telomeric region, which may have resulted from ancestral  
291 telomere damage and repair processes.

292 **TTAGAC-containing units were probably used to maintain the integrity of TTAGGC**  
293 **telomeres**

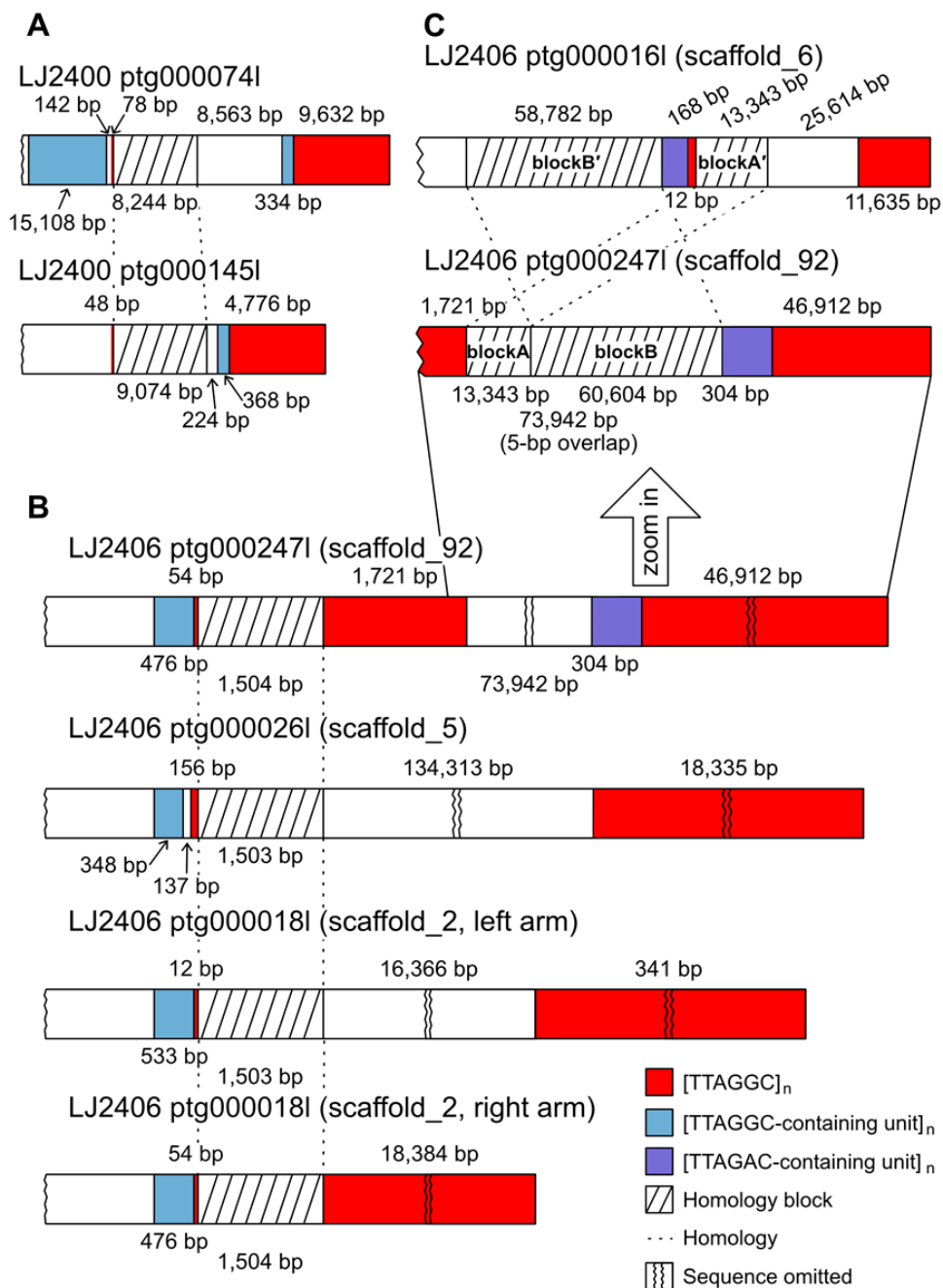
294 We postulated that the identified subtelomeric clusters of the TTAGRC-containing units and  
295 ITSs were evidence of ancestral telomere damage and repair via ALT mechanisms and that if  
296 true, this would help understand the role of TTAGRC-containing unit clusters in telomere  
297 maintenance. Among Structure 2–5, Structure 5 may be explained by BIR, one of the most  
298 well-known ALT mechanisms for telomere repair (Malkova et al. 1996; Bosco and Haber 1998;  
299 Kim et al. 2019a; Kim et al. 2020). Telomeres that have been damaged or shortened should



300 be repaired, and BIR may rely on homology between shortened telomeric repeats and ITSs at  
301 other loci (Fig. 2B, left side). The replication was then activated, and occasionally, sequences  
302 beside the ITS would also be replicated (Fig. 2B, middle). Furthermore, if the original  
303 homology block contained a TTAGRC-containing unit cluster, the cluster would also be  
304 duplicated simultaneously, resulting in a new subtelomere structure with a homology block  
305 interposed between the ITS and the TTAGRC-containing unit cluster. Finally, a new telomere  
306 composed of TTAGGC repeats could be replenished by active telomerase (Fig. 2B, right side).  
307 We then hypothesized that if Structure 5 cases in our genomes had been generated via BIR,  
308 we should be able to identify another sequence block homologous to the interposed  
309 sequence between the ITS and the TTAGRC-containing unit cluster.

310 To test this hypothesis, we searched for homology blocks in the sequences between an ITS  
311 and a TTAGRC-containing unit cluster from each of three contigs representing Structure 5 in  
312 whole genome sequences (ptg000074I and ptg000145I of LJ2400 and ptg000247I of LJ2406)  
313 (Fig. 2, Fig. 3, Supplemental Fig. S8, and Table S10). ptg000074I and ptg000145I of LJ2400  
314 shared 8-kb and 9-kb homology blocks adjacent to the ITS and had a TTAGGC-containing  
315 unit cluster ~9-kb and ~200-bp away from the shared block, respectively (Fig. 3A). These 8-  
316 kb and 9-kb homology blocks pointed to the possibility of their replication via BIR using the  
317 ITS as homology.

318



319

320

321 **Figure 3.** Traces of telomere damage and repair processes through ALT mechanisms  
 322 identified in subtelomeric regions of genome assemblies of TTAGGC-telomere isolates. (A–C)  
 323 Schematic representations of subtelomeres in the genome assemblies of LJ2400 and LJ2406.

324 Hatched boxes indicate homology blocks between two or more subtelomeres, and dashed  
325 lines indicate homologous relationships. The red boxes represent telomeric-repeat clusters.  
326 Violet and sky blue boxes represent TTAGAC-containing unit clusters and TTAGGC-  
327 containing unit clusters, respectively. Not to scale.

328

329 The ptg000247l of LJ2406 had a more evident BIR signature than the ptg000074l and  
330 ptg000145l of LJ2400, indicating that the subtelomeric TTAGGC-containing unit cluster was  
331 built via the ALT process. The subtelomeric region of ptg000247l of LJ2406 consisted of a  
332 TTAGGC-containing unit cluster, a 54-bp ITS, a 1.5-kb sequence block, a 1.7-kb ITS, a 74-kb  
333 sequence block, and a TTAGAC-containing unit cluster close to the telomeric region (Fig. 3B).  
334 By searching for this complex subtelomeric sequence in the whole genome using BLAST, we  
335 determined that the 1.5-kb and 74-kb blocks had homologous sequences in other  
336 subtelomeric regions. The 1.5-kb block between the 54-bp ITS and 1.7-kb ITS had almost  
337 identical homologous sequences in three different subtelomeric regions. These shared blocks  
338 were directly adjacent to short and variable-length ITSs near TTAGGC-containing unit  
339 clusters (Fig. 3B). The TTAGGC-containing cluster and ITS may have been utilized for  
340 homology to replicate the 1.5-kb homology blocks.

341 The 74-kb block between the 1.7-kb ITS and the TTAGAC-containing unit cluster possessed  
342 another trace of HDR and an additional replication of a TTAGGC-containing unit cluster after  
343 telomere damage (Fig. 3C). As the 1.7-kb length of the ITS is too long to be created by  
344 random mutation, it could represent evidence of ancestral telomere damage and repair. The

345 74-kb block contained at least two distinct homology blocks: the 13-kb blockA and the 61-  
346 kb blockB (Fig. 3C). The 13-kb blockA directly linked to the ITS in ptg000247l had an identical  
347 blockA' in ptg000016l that was also directly attached to another 180-bp sequence of an ITS  
348 and a TTAGAC-containing unit cluster. The 61-kb blockB was homologous but not identical  
349 to the 59-kb blockB' located on the opposite side of the 180-bp block of the ITS and the  
350 TTAGAC-containing unit cluster in ptg000016l. Of note, the last 5 bp of the 13-kb blockA and  
351 the first 5 bp of the 61-kb blockB were identical (i.e. TAAAT). The 61-kb blockB was further  
352 divided into four blocks, each of which also exhibited microhomologies with the adjacent  
353 blocks (Supplemental Fig. S10 and Supplemental Table S13). These data imply that telomere  
354 damage and repair may have occurred in the following order: first, the 13-kb blockA in  
355 ptg000247l was replicated by BIR using homology between the 1.7-kb ITS in ptg000247l and  
356 the 180-bp block of the ITS and the TTAGAC-containing unit cluster in ptg000016l. Next, the  
357 61-kb blockB in ptg000247l was replicated by multiple rounds of microhomology-mediated  
358 BIR (MMBIR) and template switching events using microhomology sequences at the end of  
359 the blocks (Supplemental Fig. S10 and Supplemental Note).

360 This 59-kb blockB' in ptg000016l was directly attached to the TTAGAC-containing unit  
361 cluster, which was duplicated in ptg000247l. Notably, the original TTAGAC-containing unit  
362 cluster in ptg000016l was shorter than the duplicated cluster in ptg000247l, implying that the  
363 duplicated cluster nearly doubled after MMBIR was completed. The duplicated TTAGAC-  
364 containing unit cluster in ptg000247l was directly linked to the TTAGGC telomere, indicating  
365 that the duplicated cluster was exposed at the end. These lines of evidence support the  
366 notion that even in TTAGGC-telomere species, TTAGAC-containing units could be

367 incorporated to constitute a telomere or at least serve as a DNA template for replenishing  
368 TRM repeats by telomerase. This use of TTAGAC-containing units in the TTAGGC-telomere  
369 isolate may have contributed to the evolution of the TTAGAC telomere from the TTAGGC  
370 telomere.

371 **Telomere-associated protein genes exhibited similar conservation patterns among**  
372 **Panagrolaimidae species/isolates**

373 We hypothesized that TTAGAC-containing unit clusters served as a component of partially  
374 stable telomere in TTAGGC-telomere species and that TBPs for TTAGGC telomere could have  
375 bound TTAGAC repeats and have been conserved in both TTAGGC-telomere and TTAGAC-  
376 telomere species. To support this hypothesis, we analyzed protein homologies in  
377 Panagrolaimidae with *B. xylophilus* as an outgroup species, in which proteins have been  
378 described to maintain or bind telomeres in *C. elegans* (Ahmed and Hodgkin 2000; Hofmann  
379 et al. 2002; Im and Lee 2003; Kim et al. 2003; Joeng et al. 2004; Im and Lee 2005; Meier et al.  
380 2006; Boerckel et al. 2007; Raices et al. 2008; Meier et al. 2009; Ferreira et al. 2013; Shtessel et  
381 al. 2013; Dietz et al. 2021; Yamamoto et al. 2021). We identified 12 proteins that exhibited  
382 similar homology patterns between TTAGGC- and TTAGAC-telomere species/isolates  
383 (Supplemental Fig. S11). In contrast, four proteins (POT-2, TEBP-2 (also known as DTN-2),  
384 HPR-9, and MRT-1) displayed inconsistent conservation patterns. POT-2 was conserved in  
385 only two of the three TTAGGC-telomere species/isolates, and TEBP-2 remained in only one of  
386 the three TTAGAC-telomere species/isolates. HPR-9 was observed in only one TTAGAC-  
387 telomere isolate. MRT-1, required for telomerase activity in *C. elegans* (Meier et al. 2009), was  
388 not detected in *B. xylophilus* or in any of the three TTAGAC-telomere species/isolates but

389 was present in all three TTAGGC-telomere species/isolates. However, MRT-1 functional  
390 domains were not conserved in the TTAGGC-telomere species/isolates. Nonetheless,  
391 homologs of the four TBPs were mostly conserved in all Panagrolaimidae species and  
392 isolates (Supplemental Table S14). Despite these variations, TRT-1 was conserved in all  
393 species and isolates, suggesting that they may have active telomerase and that changes in its  
394 RNA template may have been involved in TRM evolution (Fig. 4; see Discussion).

395

## 396 **DISCUSSION**

397 TRMs and their protein partners are well conserved and mostly co-evolving because they  
398 must be connected to maintain the DNA–protein complex, telomeres (Shakirov et al. 2009;  
399 Steinberg-Neifach and Lue 2015; Sepsiova et al. 2016; Červenák et al. 2019). Nevertheless,  
400 TRMs have evolved across several taxa (Fulnečková et al. 2013; Garavís et al. 2013; Peska and  
401 Garcia 2020; Červenák et al. 2021). In this study, we identified three novel TRMs in Nematoda  
402 and confirmed that TTAGAC, one of the three novel TRMs, composes telomeres in a subset  
403 of Panagrolaimidae isolates. We also hypothesized that TTAGAC evolved through TTAGAC-  
404 containing unit clusters and the robustness of the TTAGGC-suited TBPs to bind tandem  
405 arrays of TTAGAC repeats in a canonical TTAGGC-telomere ancestor.

406 The consistent pattern of TRM changes observed in other multicellular organisms supported  
407 our hypothesis. First, sequence changes in plant TRMs also exhibit key characteristics (Peska  
408 and Garcia 2020). In particular, the basal TRM in plants, TTTAGGG, (*Arabidopsis*-type)  
409 (Richards and Ausubel 1988) evolved into \_TTAGGG (vertebrate-type) (Weiss and Scherthan

410 2002; Sýkorová et al. 2003; Sýkorová et al. 2006), ITTTAGGG (*Chlamydomonas*-type)  
411 (Fulnečková et al. 2012), TTCAGG\_ (*Genlisea*-type) (Tran et al. 2015), ITTCAGG\_ (*Genlisea*-  
412 type) (Tran et al. 2015), ITTTAGG\_ (*Klebsormidium*-type) (Fulnečková et al. 2013), and  
413 IIIITTTAGGG (*Cestrum*-type) (Peška et al. 2015). Briefly, these variant TRMs exhibited  
414 alterations in the lengths of the T and G arms or changes in pyrimidine (T to C) nucleotides  
415 close to the middle A. Pyrimidine nucleotide conversion, rather than changes between  
416 pyrimidine and purine nucleotides and vice versa, has also been observed in insects in which  
417 TTAGG changed to TCAGG (Mravinac et al. 2011). Similarly, in the current study, TTAGGC  
418 changed to TTAGGI (pyrimidine conversion) and TTAGAC (purine conversion) in nematodes.  
419 Considering pyrimidines (T and C) have comparable base sizes and purines (G and A) are of  
420 similar sizes, we propose that conversions between pyrimidines or between purines do not  
421 sterically hinder TBP binding, allowing pre-existing TBPs to attach to the modified TRM.  
422 Furthermore, in yeasts and plants, TBPs are sufficiently robust to bind to various types of  
423 TRM despite several base pair changes (Rotková et al. 2004; Fajkus et al. 2005; Kramara et al.  
424 2010; Visacka et al. 2012; Červenák et al. 2019; Tomáška et al. 2019; Červenák et al. 2021). In  
425 yeast, a TBP binds at least six different types of TRMs, implying binding robustness of TBPs  
426 during TRM evolution (Červenák et al. 2019). Here we suggest that this idea could be further  
427 supported by TTAGAC-containing unit clusters in TTAGGC-telomere species.

428 It is still unclear whether TTAGGC-binding TBPs also bind to TTAGAC in TTAGGC-telomere  
429 Panagrolaimidae species/isolates. Traces of ALT action identified in our genome assemblies  
430 revealed that TTAGAC-containing units were used to repair telomere damage in TTAGGC-  
431 telomere isolates. Two TTAGGC-telomere isolates and one TTAGAC-telomere isolate

432 examined harbored both clusters of consecutive TTAGGC- and TTAGAC-containing units.  
433 Some clusters were attached directly or were adjacent to the telomeres. Specifically, the  
434 subtelomeric sequences of ptg000247l in LJ2406, a TTAGGC-telomere isolate, showed  
435 evidence of direct usage of a TTAGAC-containing unit for the repair of a damaged telomere.  
436 In the vicinity of a damaged and shortened telomere, there were homologous sequence  
437 blocks and a TTAGAC-containing unit cluster, which were probably replicated by BIR and  
438 MMBIR, and the TTAGAC-containing unit cluster was directly adjacent to its telomeric  
439 TTAGGC cluster. Thus, at least over a brief period of time, the TTAGAC-containing unit cluster  
440 was exposed at the end of the chromosome before the TTAGGC repeats were replenished.  
441 Furthermore, the TTAGAC-containing unit cluster was not only duplicated but also elongated  
442 at the end because it was nearly twice as long as its initial cluster template in a separate  
443 subtelomeric region. This cluster might have been elongated via replication slippage based  
444 on its repetitive nature or via ALT mechanisms that can replicate TRM-containing units at the  
445 end of the chromosome. We could not determine the specific mechanisms involved in the  
446 elongation of the TTAGAC-containing unit cluster. If the elongation was achieved via ALT  
447 mechanisms, this suggests that the TTAGAC-containing unit cluster exhibits its own  
448 replication capability in the telomeric region to maintain the telomere.  
449 If the TTAGAC-containing unit cluster acted as a component of the telomere, the TTAGGC-  
450 suited TBPs would bind to the telomere; otherwise, the end would be recognized as a DNA  
451 damage site. This binding robustness of TBPs, if it exists as reported in fungi, may explain the  
452 subtelomere structure and TRM evolution. This robustness could be achieved via two  
453 potential ways: (1) the TTAGGC-suited TBPs also exhibited sufficient binding affinity for

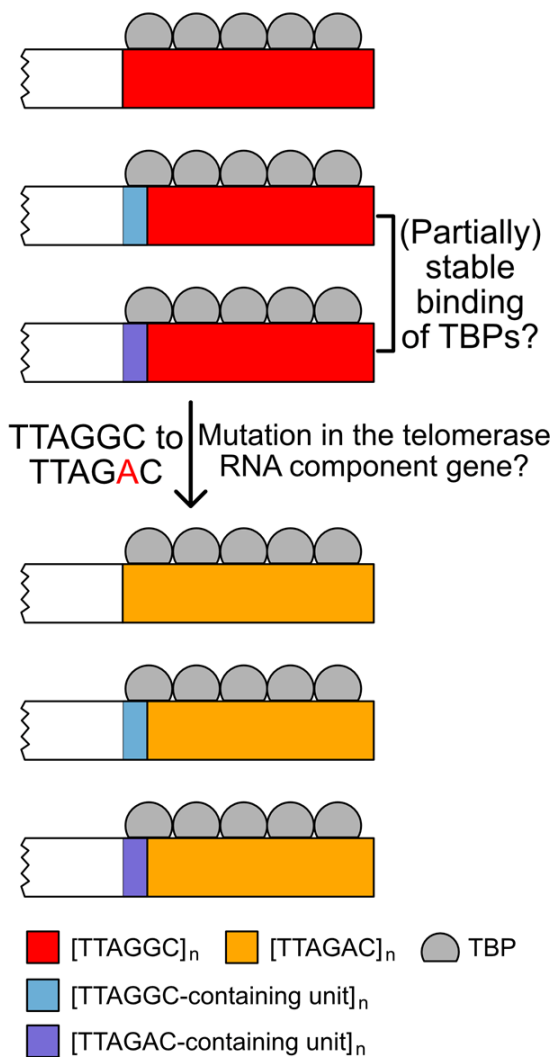


454 TTAGAC, such that TTAGAC-unit clusters could be utilized for repairing telomere damage.  
455 This binding affinity stabilized the TTAGAC-containing unit–TBP complex as a telomere. (2)  
456 TBPs exhibited a weak binding affinity to TTAGAC and formed a partially stable telomere  
457 complex, and the affinity strengthened through frequent use of TTAGAC-containing unit  
458 clusters to repair telomere damage and ensure fitness. In both cases, TTAGGC-suited TBPs  
459 could also stabilize TTAGAC telomeres, which thus facilitated the conversion from TTAGGC  
460 telomeres to TTAGAC telomeres.

461 Our results suggest a plausible evolutionary model for the TRM conversion in the family  
462 Panagrolaimidae. First, ancestral TTAGGC-telomere species may have utilized various ALT  
463 mechanisms to counteract telomere damage when active telomerase cannot access the  
464 damaged telomere (Fig. 4). Replication of TTAGGC-containing unit clusters could represent  
465 one such ALT mechanism and would have been used to repair damaged telomeres.  
466 Consequently, active telomerase may use unit clusters as a starting template to fully  
467 replenish the partially repaired telomere. Because TBPs can fully or partially stabilize  
468 telomere complexes consisting of TTAGAC-containing unit clusters, the evolution of the TRM  
469 conversion to TTAGAC had a greater fitness than other TTAGGC variants. We could not  
470 identify the telomerase RNA component gene in Panagrolaimidae. However, conservation of  
471 TRT-1 and highly accurate replication of TRMs at the telomere probably support the  
472 presence of an active telomerase in these species/isolates (Fig. 1G and Supplemental Fig. S6  
473 and S11). TRM would have converted to TTAGAC via mutation in the telomerase RNA  
474 component gene, leading to TTAGAC telomeres, although it remains unclear whether this  
475 change involved a single mutation in the gene or coexistence of the original and mutated

476 genes. This transition may have occurred long ago, since TTAGAC- and TTAGGC-telomere  
 477 isolates had only TTAGAC- and TTAGGC-ITSs, respectively. Moreover, both telomeres and  
 478 ITSs consisted of the same TRM, and sequences of their ITSs were not much degenerated,  
 479 indicating that these ITSs resulted from recent, and probably frequent, telomere damage  
 480 events in these isolates.

481



482

483

484 **Figure 4.** A model for TRM evolution in Panagrolaimidae. If TBPs with affinity for TTAGGC  
485 telomeres could bind to any of the TTAGGC telomere, TTAGGC-containing unit clusters, or  
486 TTAGAC-containing unit clusters, they were able to construct a fully or partially stable  
487 telomere. This binding robustness of TBPs may have facilitated the TRM conversion from  
488 TTAGGC to TTAGAC. Even after TRM changed via mutation of the telomerase RNA  
489 component gene, if it occurred, TBPs could still bind to altered telomeric repeats, which  
490 possibly contributed to the evolution of a novel TRM, TTAGAC, in the Panagrolaimidae  
491 family.

492

493 It is unclear whether TTAGGC-suited TBPs could bind to the novel telomeric sequence;  
494 however, if this were possible, the TTAGAC cluster–TBP complex would be partially stabilized,  
495 preventing the new telomere from being recognized as a DNA damage site. This hypothesis  
496 can be evaluated directly by inducing a mutation in the telomerase RNA component gene  
497 and then measuring the robustness of TBP in terms of sequence specificity. Unfortunately,  
498 we could not identify the telomerase RNA component gene for these isolates, as the gene  
499 has not been identified even in *C. elegans*. Further studies are required to support our  
500 hypothesis. Nonetheless, we identified TTAGGC- and/or TTAGGT-containing unit clusters in  
501 putative subtelomeric regions of *Caenorhabditis uteleia*, which suggests that TRM-containing  
502 unit clusters are associated with telomere maintenance and that their usage in telomere  
503 maintenance contributes to TRM evolution (see also Supplemental Note).

504 Our results describe the independent evolution of three novel TRMs in Nematoda. We found  
505 that an ALT-mediated mechanism may have been used to repair ancestral telomere damage  
506 in Panagrolaimidae nematodes. Further, we hypothesized that the use of TTAGAC-containing  
507 units and the robustness of TBPs facilitated the evolution of the novel TRM. As the  
508 robustness of the TBPs may depend on the same-sized bases between canonical and novel  
509 TRMs, the evolutionary path we propose for Panagrolaimidae can also be applied to plants,  
510 insects, or other nematodes where mutations occur only between pyrimidine nucleotides or  
511 between purine nucleotides. Although our study cannot explain all TRM changes in  
512 Nematoda, it provides new insight into telomere evolution through ALT and the robustness  
513 of TBPs.

514

## 515 **METHODS**

### 516 **Worm sampling and culture**

517 Nematodes were collected from rotten fruits in the Republic of Korea (see Supplemental  
518 Table S5 for more information). They were grown in plates containing nematode growth  
519 medium seeded with *Escherichia coli* strain OP50 and contaminated by their natural  
520 microbes.

### 521 **DNA/RNA extraction and sequencing**

522 Mixed-stage worms were lysed, and genomic DNA was extracted using the Gentra Puregene  
523 Cell and Tissue Kit (QIAGEN) to obtain WGS data for Panagrolaimidae isolates, LJ2281,

524 LJ2284, LJ2285, LJ2400, LJ2402, and LJ2406. Macrogen (South Korea,  
525 <https://www.macrogen.com/en/main>) prepared DNA sequencing libraries using TruSeq Nano  
526 DNA and performed 151-bp paired-end DNA sequencing on the Illumina NovaSeq 6000  
527 platform. One adult female worm was lysed, and its genomic DNA was amplified in the same  
528 0.2-mL PCR tube using the REPLI-g single-cell WGA kit (QIAGEN) to obtain single-worm WGS  
529 data from LJ2050, LJ2051, LJ2060, LJ2070, LJ2072, LJ2401, LJ2411, and LJ2417. Paired-end  
530 DNA sequencing was performed using the Illumina NovaSeq 6000 platform by Theragen Bio  
531 (South Korea, <https://www.theragenbio.com/en/>).

532 Long-read DNA sequencing and short-read RNA sequencing of LJ2284, LJ2285, LJ2400, and  
533 LJ2406 were conducted as described by Kim et al. (Kim et al. 2019a) and Lee et al. (Lee et al.  
534 2022a). In summary, genomic DNA was extracted from mixed-stage worms using  
535 phenol/chloroform/isoamyl alcohol (25:24:1) and sequenced using the HiFi mode of the  
536 PacBio Sequel II platform by Macrogen. RNA was extracted from mixed-stage worms using  
537 the TRIzol method. RNA sequencing libraries were prepared using TruSeq Nano DNA and  
538 sequenced by Macrogen using the Illumina NovaSeq 6000 platform with paired-end reads.

### 539 **Preparing publicly available WGS data**

540 We included Nematoda species in our study, whose genome assembly data were available in  
541 the GenBank database and short-read sequencing data were available in the NCBI Sequence  
542 Read Archive (SRA) (RRID:SCR\_004891). The following criteria were used to filter the short-  
543 read sequencing data: Instrument, *Illumina* (if HiSeq data were available, we used HiSeq;  
544 otherwise, MiSeq, NextSeq, and Genome Analyzer II data were selected); Source, *Genomic*;

545 Layout, *PAIRED*; Number of Bases, >5 Gb; Spot number, >5 million; Read length, >70 bp.  
546 Nematode clades were classified according to the phylogenetic tree (Smythe et al. 2019). Any  
547 genus that was not included in the phylogenetic tree was excluded. WGS data for *Enoplus*  
548 *brevis*, which lacked genome assembly information in the GenBank database, and WGS data  
549 for *Panagrellus redivivus* (Srinivasan et al. 2013) that was supplied by Dr. P. W. Sternberg  
550 (now it can be accessible via NCBI SRA under accession number SRR25684730) were added  
551 to the filtered datasets. Detailed accession information is available in Supplemental Tables S1  
552 and S2.

### 553 **Identifying TRMs using short-read WGS data**

554 To normalize the public WGS data, we trimmed all reads to 60 bp and used only 5 million  
555 sub-sampled reads from the R1 files using Seqtk (<https://github.com/lh3/seqtk>) (version 1.3-  
556 r106; `seqtk sample -s 11 - 5000000`). For each dataset, 23-mers were counted using Kounta  
557 (<https://github.com/tseemann/kounta>) (version 0.2.3; `kounta --kmer 23 --out`). Only tandemly  
558 repeated sequences with unit lengths of 5–7 bp and counts >99 were used to identify  
559 putative TRMs that were most frequent and most similar to the canonical TTAGGC sequence.  
560 Methods used to further validate the novel putative TRMs are described in Supplemental  
561 Methods. We averaged the counts of the 23-mers that contained the corresponding TRM  
562 concatemers to compare the number of TRMs across species. For the Panagrolaimidae  
563 isolates, we used 20 million sub-sampled reads and all 23-mers, as telomeric repeats were  
564 not evenly amplified during whole-genome amplification.

### 565 **Genome assembly**

566 HiFi reads were *de novo* assembled using Hifiasm (Cheng et al. 2021) (version 0.13-r308;  
567 *hifiasm -l0*). Contigs that were potentially contaminated with bacterial sequences were  
568 removed as described by Kim et al. (Kim et al. 2019a). Scaffolding and visualization based on  
569 the Hi-C data are described in Supplemental Methods. The completeness of the genome  
570 assembly was evaluated using BUSCO (Simão et al. 2015) (version 4.0.6; *busco -m genome -l*  
571 *nematoda\_odb10*) with the nematoda dataset in the OrthoDB release 10. Isolate-specific  
572 repetitive sequences were identified using BuildDatabase (Flynn et al. 2020) (version 2.0.1;  
573 default options) and RepeatModeler (Flynn et al. 2020) (version 2.0.1; *RepeatModeler -*  
574 *database -LTRStruct*). Isolate-specific and known metazoan-repetitive sequences were  
575 masked using RepeatMasker (Chen 2004) (version 4.1.0; *RepeatMasker -lib -s* for species-  
576 specific repeats and *RepeatMasker -species metazoa -s* for metazoan repeats). We mapped  
577 the RNA-seq reads to the repeat-masked genome using HISAT2 (Kim et al. 2019b) (version  
578 2.2.1; *hisat2-build* for genome indexing and *hisat2* with default options to map the RNA-seq  
579 reads to the corresponding genome). RNA-mapping data was used to annotate genes using  
580 BRAKER (Stanke et al. 2006; Stanke et al. 2008; Li et al. 2009; Barnett et al. 2011; Lomsadze et  
581 al. 2014; Buchfink et al. 2015; Hoff et al. 2016; Hoff et al. 2019; Bruna et al. 2021) (version  
582 2.1.5; *braker.pl --genome -bam --softmasking*).

### 583 **Preparation of 18S ribosomal DNA sequences to generate the Panagrolaimidae** 584 **phylogenetic tree**

585 For *Panagrolaimus* sp. PS1159, *Panagrolaimus davidi*, *Panagrellus redivivus*, and  
586 *Bursaphelenchus xylophilus*, we used publicly available 18S rDNA sequences (GenBank  
587 accessions: U81579.1, AJ567385.1, AF083007.1, and KJ636306.1, respectively). For the HiFi-

588 based *de novo* genome assemblies, we extracted 18S rDNA sequences by searching known  
589 nematode 18S rDNA PCR primers (nSSU\_F\_04: 5'-GCTTGTCTCAAAGATTAAGCC-3' (Blaxter et  
590 al. 1998) and nSSU\_R\_82: 5'-TGATCCTTCTGCAGGTTACCTAC-3' (Medlin et al. 1988)) in  
591 genome assemblies using BLAST+ (Camacho et al. 2009) (version 2.7.1; *makeblastdb -*  
592 *input\_type fasta -dbtype nucl* and *blastn -task blastn-short -outfmt 6*).

593 For the other TTAGAC-TRM isolates used in this study, we mapped their short-read DNA  
594 sequencing data to the LJ2285 genome assembly using BWA-MEM (version 0.7.17; *bwa*  
595 *mem*, default option), and the 18S rDNA sequence variation of each isolate were identified  
596 using BCFtools (Li 2011a) (version 1.13; *bcftools mpileup -Ou -f | bcftools call -Ou -mv |*  
597 *bcftools norm -f -Oz -o*). The indexed output VCF files were obtained using Tabix (Li 2011b)  
598 (version 1.13; default option), and the LJ2285 18S rDNA sequence was replaced with their  
599 variants of each isolate using SAMtools (Li et al. 2009) (version 1.13) and BCFtools (*samtools*  
600 *faidx -r | bcftools consensus -o*). For the other TTAGGC-TRM isolates, we used the LJ2400  
601 genome assembly as a reference and repeated the procedure described above. All 18S rDNA  
602 sequences of Panagrolaimidae obtained in this study are listed in Supplemental Table S6. We  
603 generated an alignment file using all 18S rDNA sequences as input for Clustal Omega  
604 (<https://www.ebi.ac.uk/Tools/msa/clustalo/>, RRID:SCR\_001591, (Sievers and Higgins 2021))  
605 (Sequence Type: DNA; Output Alignment Format: PHYLIP). We used this alignment as an  
606 input to RAxML (Stamatakis 2014) (version 8.2.12) using raxmlGUI 2.0 (Edler et al. 2021)  
607 (version 2.0.10; options: GTRGAMMA and ML+rapid bootstrap with 1000 replications) to  
608 infer the phylogenetic relationships, which were visualized using Dendroscope (Huson and  
609 Scornavacca 2012) (version 3.8.4).



## 610 **Telomere and subtelomere structure in the genome assemblies**

611 We selected candidate telomere-containing contigs using two tandemly repeated copies of  
612 TTAGRC that appeared  $\geq 3$  times in the 600-bp region at each end of the contig. We  
613 manually validated these telomeric regions using the following criteria: TRM cluster length  
614  $\geq 500$  bp (the longest ITS length in *C. elegans*) (Yoshimura et al. 2019) or TRM cluster still  
615 located at the end after scaffolding (only for LJ2284 and LJ2406). We analyzed whether each  
616 telomere-containing contig/scaffold had clusters with  $\geq 6$  copies of TRMs or whether  
617 TTAGRC-containing units repeated tandemly in its subtelomeric region (up to 200 kb from  
618 the end of the contig/scaffold). For LJ2285, we considered sequences consisting of 5–9  
619 copies of different units that contained TTAGRC and similar sequences as unit clusters  
620 because LJ2285 did not contain clusters composed of the same units. Subsequently, we  
621 investigated whether the unit cluster (containing  $\geq 6$  copies of units, the same TTAGRC and  
622 identity  $\geq 85\%$  of units) existed outside the subtelomeric region of telomere-containing  
623 contigs/scaffolds using BLAST+ (Camacho et al. 2009) (version 2.12.0; *makeblastdb -*  
624 *input\_type fasta -dbtype nucl; blastn -task blastn-short -outfmt 6* for sequences  $< 30$  bp and  
625 *blastn -task megablast -outfmt* for sequences  $\geq 30$  bp). Unit sequences of LJ2284, LJ2400, and  
626 LJ2406 and unit cluster sequences in LJ2285 were denoted starting with TTAGRC  
627 (Supplemental Table S12). The BIR traces were analyzed by searching for homologous  
628 sequences between ITSs, TTAGRC-containing unit clusters, or telomeric repeats against their  
629 corresponding genome assembly using BLAST+ (Camacho et al. 2009) (version 2.7.1;  
630 *makeblastdb -input\_type fasta -dbtype nucl and blastn -task megablast -outfmt 6*).

## 631 **Conservation analysis of telomere-associated proteins**

632 Protein FASTA sequences were downloaded from WormBase for *C. elegans* (Release WS281)  
633 and WormBase ParaSite (Howe et al. 2017) for *Panagrolaimus* sp. PS1159, *Panagrolaimus*  
634 *dauidi*, *Panagrellus redivivus*, and *B. xylophilus* (Release WBPS15). Protein sequences for  
635 *Panagrolaimus* sp. PS1579 and *Panagrolaimus* sp. ES5 were not publicly available. For the  
636 four Panagrolaimidae isolates (LJ2284, LJ2285, LJ2400, and LJ2406), we used protein FASTA  
637 sequences obtained through gene annotation using BRAKER. For the non-*C. elegans*  
638 nematodes, we searched for protein sequences that were conserved in *C. elegans* using  
639 DIAMOND (Buchfink et al. 2021) (version 2.0.11; *diamond blastp -d -q -o --threads 20 --very-*  
640 *sensitive* and *diamond blastp -d -q -o --threads 20 --ultra-sensitive*) to characterize telomere-  
641 associated protein sequences that included TRT-1, POT-1, POT-2, POT-3, MRT-1, MRT-2,  
642 TEBP-1 (also known as DTN-1), TEBP-2 (also known as DTN-2), HPR-9, HPR-17, HUS-1, SUN-  
643 1, CEH-37, HMG-5, HRP-1, and PLP-1. We filtered the nematode's highest bit score protein  
644 sequence for each *C. elegans* telomere-associated protein and identified the conserved  
645 domains using NCBI CD-search (Marchler-Bauer and Bryant 2004; Lu et al. 2020) (CDD  
646 database, version 3.19).

647

## 648 DATA ACCESS

649 Raw sequencing data and genome assemblies have been submitted in the NCBI BioProject  
650 database (<https://www.ncbi.nlm.nih.gov/bioproject>) under the accession number  
651 PRJNA845886 and in the Korean Nucleotide Archive (KoNA, <https://kobic.re.kr/kona>) under  
652 the BioProject accession number KAP220348 (sequencing data only).

653

654 **COMPETING INTEREST STATEMENT**

655 None declared.

656

657 **ACKNOWLEDGEMENTS**

658 This study was supported by Samsung Science and Technology Foundation [SSTF-BA1501-  
659 52]; and National Research Foundation of Korea [2019R1A6A1A10073437 to J.K.]. J. Lim was  
660 also supported by a scholarship for basic research, Seoul National University. We thank Dr. P.  
661 W. Sternberg for providing and publishing valuable sequencing data of *Panagrellus redivivus*  
662 and are grateful to the Darwin Tree of Life Project Consortium for releasing sequencing data  
663 of *Caenorhabditis uteleia*. We also thank Namhee Kim and Sungyeol Ahn for providing  
664 accession to their farms to collect rotten fruits and Dr. D. S. Lim for collaboration in collection  
665 of nematode species. We appreciate Dr. S. Sung for providing the suggestions on generating  
666 Hi-C library, and Dr. C. Kim for the help in Hi-C data processing.

667

668 **AUTHOR CONTRIBUTIONS**

669 Jiseon Lim: Conceptualization, Methodology, Formal Analysis, Investigation, Writing-Original  
670 Draft, Writing-Review & Editing. Wonjoo Kim: Investigation. Jun Kim: Conceptualization,  
671 Methodology, Investigation, Writing-Original Draft, Writing-Review & Editing. Junho Lee:  
672 Conceptualization, Writing-Review & Editing, Funding Acquisition, Supervision.

673

674 **REFERENCES**

- 675 Abad JP, De Pablos B, Osoegawa K, De Jong PJ, Martín-Gallardo A, Villasante A. 2004. TAHRE,  
676 a novel telomeric retrotransposon from *Drosophila melanogaster*, reveals the origin  
677 of *Drosophila* telomeres. *Molecular biology and evolution* **21**: 1620-1624.
- 678 Ahmed S, Hodgkin J. 2000. MRT-2 checkpoint protein is required for germline immortality  
679 and telomere replication in *C. elegans*. *Nature* **403**: 159-164.
- 680 Barnett DW, Garrison EK, Quinlan AR, Strömberg MP, Marth GT. 2011. BamTools: a C++ API  
681 and toolkit for analyzing and managing BAM files. *Bioinformatics* **27**: 1691-1692.
- 682 Blaxter ML, De Ley P, Garey JR, Liu LX, Scheldeman P, Vierstraete A, Vanfleteren JR, Mackey  
683 LY, Dorris M, Frisse LM. 1998. A molecular evolutionary framework for the phylum  
684 Nematoda. *Nature* **392**: 71-75.
- 685 Boerckel J, Walker D, Ahmed S. 2007. The *Caenorhabditis elegans* Rad17 homolog HPR-17 is  
686 required for telomere replication. *Genetics* **176**: 703-709.
- 687 Bosco G, Haber JE. 1998. Chromosome break-induced DNA replication leads to nonreciprocal  
688 translocations and telomere capture. *Genetics* **150**: 1037-1047.
- 689 Brůna T, Hoff KJ, Lomsadze A, Stanke M, Borodovsky M. 2021. BRAKER2: automatic  
690 eukaryotic genome annotation with GeneMark-EP+ and AUGUSTUS supported by a  
691 protein database. *NAR genomics and bioinformatics* **3**: lqaa108.
- 692 Bryan TM, Englezou A, Gupta J, Bacchetti S, Reddel R. 1995. Telomere elongation in immortal  
693 human cells without detectable telomerase activity. *The EMBO journal* **14**: 4240-4248.
- 694 Buchfink B, Reuter K, Drost H-G. 2021. Sensitive protein alignments at tree-of-life scale using  
695 DIAMOND. *Nature methods* **18**: 366-368.
- 696 Buchfink B, Xie C, Huson DH. 2015. Fast and sensitive protein alignment using DIAMOND.  
697 *Nature methods* **12**: 59-60.
- 698 The *C. elegans* Sequencing Consortium. 1998. Genome sequence of the nematode *C.*  
699 *elegans*: a platform for investigating biology. *Science* **282**: 2012-2018.
- 700 Camacho C, Coulouris G, Avagyan V, Ma N, Papadopoulos J, Bealer K, Madden TL. 2009.  
701 BLAST+: architecture and applications. *BMC bioinformatics* **10**: 1-9.
- 702 Červenák F, Jurikova K, Devillers H, Kaffe B, Khatib A, Bonnell E, Sopkovičová M, Wellinger RJ,  
703 Nosek J, Tzfati Y. 2019. Identification of telomerase RNAs in species of the *Yarrowia*  
704 clade provides insights into the co-evolution of telomerase, telomeric repeats and  
705 telomere-binding proteins. *Scientific reports* **9**: 1-15.
- 706 Červenák F, Sepšiová R, Nosek J, Tomáška L. 2021. Step-by-step evolution of telomeres:  
707 lessons from yeasts. *Genome biology and evolution* **13**: evaa268.
- 708 Chen N. 2004. Using Repeat Masker to identify repetitive elements in genomic sequences.  
709 *Current protocols in bioinformatics* **5**: 4.10. 11-14.10. 14.
- 710 Cheng H, Concepcion GT, Feng X, Zhang H, Li H. 2021. Haplotype-resolved de novo  
711 assembly using phased assembly graphs with hifiasm. *Nature methods* **18**: 170-175.

- 712 The Darwin Tree of Life Project Consortium. 2022. Sequence locally, think globally: The  
713 Darwin tree of life project. *Proceedings of the National Academy of Sciences* **119**:  
714 e2115642118.
- 715 Dayi M, Sun S, Maeda Y, Tanaka R, Yoshida A, Tsai IJ, Kikuchi T. 2020. Nearly complete  
716 genome assembly of the pinewood nematode *Bursaphelenchus xylophilus* strain  
717 Ka4C1. *Microbiology resource announcements* **9**: e01002-01020.
- 718 De Lange T. 2009. How telomeres solve the end-protection problem. *Science* **326**: 948-952.
- 719 Dietz S, Almeida MV, Nischwitz E, Schreier J, Viceconte N, Fradera-Sola A, Renz C, Ceron-  
720 Noriega A, Ulrich HD, Kappei D. 2021. The double-stranded DNA-binding proteins  
721 TEBP-1 and TEBP-2 form a telomeric complex with POT-1. *Nature communications* **12**:  
722 1-20.
- 723 Edler D, Klein J, Antonelli A, Silvestro D. 2021. raxmlGUI 2.0: a graphical interface and toolkit  
724 for phylogenetic analyses using RAxML. *Methods in Ecology and Evolution* **12**: 373-  
725 377.
- 726 Fajkus J, Sýkorová E, Leitch AR. 2005. Telomeres in evolution and evolution of telomeres.  
727 *Chromosome Research* **13**: 469-479.
- 728 Ferreira HC, Towbin BD, Jegou T, Gasser SM. 2013. The shelterin protein POT-1 anchors  
729 *Caenorhabditis elegans* telomeres through SUN-1 at the nuclear periphery. *Journal of*  
730 *cell biology* **203**: 727-735.
- 731 Flynn JM, Hubley R, Goubert C, Rosen J, Clark AG, Feschotte C, Smit AF. 2020.  
732 RepeatModeler2 for automated genomic discovery of transposable element families.  
733 *Proceedings of the National Academy of Sciences* **117**: 9451-9457.
- 734 Fulnečková J, Hasíková T, Fajkus J, Lukešova A, Eliaš M, Sýkorova E. 2012. Dynamic evolution  
735 of telomeric sequences in the green algal order Chlamydomonadales. *Genome*  
736 *biology and evolution* **4**: 248-264.
- 737 Fulnečková J, Ševčíková T, Fajkus J, Lukešova A, Lukeš M, Vlček Č, Lang BF, Kim E, Eliaš M,  
738 Sýkorova E. 2013. A broad phylogenetic survey unveils the diversity and evolution of  
739 telomeres in eukaryotes. *Genome biology and evolution* **5**: 468-483.
- 740 Garavís M, Gonzalez C, Villasante A. 2013. On the origin of the eukaryotic chromosome: the  
741 role of noncanonical DNA structures in telomere evolution. *Genome biology and*  
742 *evolution* **5**: 1142-1150.
- 743 Heaphy CM, Subhawong AP, Hong S-M, Goggins MG, Montgomery EA, Gabrielson E, Netto  
744 GJ, Epstein JI, Lotan TL, Westra WH. 2011. Prevalence of the alternative lengthening of  
745 telomeres telomere maintenance mechanism in human cancer subtypes. *The*  
746 *American journal of pathology* **179**: 1608-1615.
- 747 Hoff KJ, Lange S, Lomsadze A, Borodovsky M, Stanke M. 2016. BRAKER1: unsupervised RNA-  
748 Seq-based genome annotation with GeneMark-ET and AUGUSTUS. *Bioinformatics* **32**:  
749 767-769.
- 750 Hoff KJ, Lomsadze A, Borodovsky M, Stanke M. 2019. Whole-genome annotation with  
751 BRAKER. In *Gene prediction*, pp. 65-95. Springer.
- 752 Hofmann ER, Milstein S, Boulton SJ, Ye M, Hofmann JJ, Stergiou L, Gartner A, Vidal M,  
753 Hengartner MO. 2002. *Caenorhabditis elegans* HUS-1 is a DNA damage checkpoint  
754 protein required for genome stability and EGL-1-mediated apoptosis. *Current biology*  
755 **12**: 1908-1918.

- 756 Howe KL, Bolt BJ, Shafie M, Kersey P, Berriman M. 2017. WormBase ParaSite– a  
757 comprehensive resource for helminth genomics. *Molecular and biochemical*  
758 *parasitology* **215**: 2-10.
- 759 Huson DH, Scornavacca C. 2012. Dendroscope 3: an interactive tool for rooted phylogenetic  
760 trees and networks. *Systematic biology* **61**: 1061-1067.
- 761 Im SH, Lee J. 2003. Identification of HMG-5 as a double-stranded telomeric DNA-binding  
762 protein in the nematode *Caenorhabditis elegans*. *FEBS letters* **554**: 455-461.
- 763 Im SH, Lee J. 2005. PLP-1 binds nematode double-stranded telomeric DNA. *Molecules & Cells*  
764 (*Springer Science & Business Media BV*) **20**.
- 765 Joeng KS, Song EJ, Lee K-J, Lee J. 2004. Long lifespan in worms with long telomeric DNA.  
766 *Nature genetics* **36**: 607-611.
- 767 Kim C, Kim J, Kim S, Cook DE, Evans KS, Andersen EC, Lee J. 2019a. Long-read sequencing  
768 reveals intra-species tolerance of substantial structural variations and new  
769 subtelomere formation in *C. elegans*. *Genome research* **29**: 1023-1035.
- 770 Kim C, Sung S, Kim J-S, Lee H, Jung Y, Shin S, Kim E, Seo JJ, Kim J, Kim D. 2021a. Telomeres  
771 reforged with non-telomeric sequences in mouse embryonic stem cells. *Nature*  
772 *communications* **12**: 1-15.
- 773 Kim C, Sung S, Kim J, Lee J. 2020. Repair and reconstruction of telomeric and subtelomeric  
774 regions and genesis of new telomeres: implications for chromosome evolution.  
775 *Bioessays* **42**: 1900177.
- 776 Kim D, Paggi JM, Park C, Bennett C, Salzberg SL. 2019b. Graph-based genome alignment and  
777 genotyping with HISAT2 and HISAT-genotype. *Nature biotechnology* **37**: 907-915.
- 778 Kim E, Kim J, Kim C, Lee J. 2021b. Long-read sequencing and de novo genome assemblies  
779 reveal complex chromosome end structures caused by telomere dysfunction at the  
780 single nucleotide level. *Nucleic acids research* **49**: 3338-3353.
- 781 Kim SH, Hwang SB, Chung IK, Lee J. 2003. Sequence-specific binding to telomeric DNA by  
782 CEH-37, a homeodomain protein in the nematode *Caenorhabditis elegans*. *Journal of*  
783 *Biological Chemistry* **278**: 28038-28044.
- 784 Kramara J, Osia B, Malkova A. 2018. Break-induced replication: the where, the why, and the  
785 how. *Trends in Genetics* **34**: 518-531.
- 786 Kramara J, Willcox S, Gunisova S, Kinsky S, Nosek J, Griffith JD, Tomaska L. 2010. Tay1 protein,  
787 a novel telomere binding factor from *Yarrowia lipolytica*. *Journal of Biological*  
788 *Chemistry* **285**: 38078-38092.
- 789 Lazzerini-Denchi E, Sfeir A. 2016. Stop pulling my strings—what telomeres taught us about  
790 the DNA damage response. *Nature reviews Molecular cell biology* **17**: 364-378.
- 791 Lee BY, Kim J, Lee J. 2022a. Intraspecific de novo gene birth revealed by presence–absence  
792 variant genes in *Caenorhabditis elegans*. *NAR Genomics and Bioinformatics* **4**:  
793 lqac031.
- 794 Lee BY, Kim J, Lee J. 2022b. Long-read sequencing infers a mechanism for copy number  
795 variation of template for alternative lengthening of telomeres in a wild *C. elegans*  
796 strain. *microPublication Biology*.
- 797 Li H. 2011a. A statistical framework for SNP calling, mutation discovery, association mapping  
798 and population genetical parameter estimation from sequencing data. *Bioinformatics*  
799 **27**: 2987-2993.

- 800 Li H. 2011b. Tabix: fast retrieval of sequence features from generic TAB-delimited files.  
801 *Bioinformatics* **27**: 718-719.
- 802 Li H, Handsaker B, Wysoker A, Fennell T, Ruan J, Homer N, Marth G, Abecasis G, Durbin R.  
803 2009. The sequence alignment/map format and SAMtools. *Bioinformatics* **25**: 2078-  
804 2079.
- 805 Lomsadze A, Burns PD, Borodovsky M. 2014. Integration of mapped RNA-Seq reads into  
806 automatic training of eukaryotic gene finding algorithm. *Nucleic acids research* **42**:  
807 e119-e119.
- 808 Lu S, Wang J, Chitsaz F, Derbyshire MK, Geer RC, Gonzales NR, Gwadz M, Hurwitz DI,  
809 Marchler GH, Song JS. 2020. CDD/SPARCLE: the conserved domain database in 2020.  
810 *Nucleic acids research* **48**: D265-D268.
- 811 Lundblad V, Blackburn EH. 1993. An alternative pathway for yeast telomere maintenance  
812 rescues est1– senescence. *Cell* **73**: 347-360.
- 813 Lydeard JR, Jain S, Yamaguchi M, Haber JE. 2007. Break-induced replication and telomerase-  
814 independent telomere maintenance require Pol32. *Nature* **448**: 820-823.
- 815 Malkova A, Ivanov EL, Haber JE. 1996. Double-strand break repair in the absence of RAD51 in  
816 yeast: a possible role for break-induced DNA replication. *Proceedings of the National*  
817 *Academy of Sciences* **93**: 7131-7136.
- 818 Marchler-Bauer A, Bryant SH. 2004. CD-Search: protein domain annotations on the fly.  
819 *Nucleic acids research* **32**: W327-W331.
- 820 Medlin L, Elwood HJ, Stickel S, Sogin ML. 1988. The characterization of enzymatically  
821 amplified eukaryotic 16S-like rRNA-coding regions. *Gene* **71**: 491-499.
- 822 Meier B, Barber LJ, Liu Y, Shtessel L, Boulton SJ, Gartner A, Ahmed S. 2009. The MRT-1  
823 nuclease is required for DNA crosslink repair and telomerase activity in vivo in  
824 *Caenorhabditis elegans*. *The EMBO journal* **28**: 3549-3563.
- 825 Meier B, Clejan I, Liu Y, Lowden M, Gartner A, Hodgkin J, Ahmed S. 2006. trt-1 is the  
826 *Caenorhabditis elegans* catalytic subunit of telomerase. *PLoS Genetics* **2**: e18.
- 827 Mravinac B, Meštrović N, Čavrak VV, Plohl M. 2011. TCAGG, an alternative telomeric  
828 sequence in insects. *Chromosoma* **120**: 367-376.
- 829 Peška V, Fajkus P, Fojtová M, Dvořáčková M, Hapala J, Dvořáček V, Polanská P, Leitch AR,  
830 Sýkorová E, Fajkus J. 2015. Characterisation of an unusual telomere motif  
831 (TTTTTtaggg) n in the plant *Cestrum elegans* (Solanaceae), a species with a large  
832 genome. *The Plant Journal* **82**: 644-654.
- 833 Peska V, Garcia S. 2020. Origin, diversity, and evolution of telomere sequences in plants.  
834 *Frontiers in plant science* **11**: 117.
- 835 Raices M, Verdun RE, Compton SA, Haggblom CI, Griffith JD, Dillin A, Karlseder J. 2008. *C.*  
836 *elegans* telomeres contain G-strand and C-strand overhangs that are bound by  
837 distinct proteins. *Cell* **132**: 745-757.
- 838 Richards EJ, Ausubel FM. 1988. Isolation of a higher eukaryotic telomere from *Arabidopsis*  
839 *thaliana*. *Cell* **53**: 127-136.
- 840 Rotková G, Skleničková M, Dvořáčková M, Sýkorová E, Leitch AR, Fajkus J. 2004. An  
841 evolutionary change in telomere sequence motif within the plant section Asparagales  
842 had significance for telomere nucleoprotein complexes. *Cytogenetic and Genome*  
843 *Research* **107**: 132-138.

- 844 Roumelioti FM, Sotiriou SK, Katsini V, Chiourea M, Halazonetis TD, Gagos S. 2016. Alternative  
845 lengthening of human telomeres is a conservative DNA replication process with  
846 features of break-induced replication. *EMBO reports* **17**: 1731-1737.
- 847 Seo B, Kim C, Hills M, Sung S, Kim H, Kim E, Lim DS, Oh H-S, Choi RMJ, Chun J. 2015.  
848 Telomere maintenance through recruitment of internal genomic regions. *Nature*  
849 *communications* **6**: 1-10.
- 850 Sepsiova R, Necasova I, Willcox S, Prochazkova K, Gorilak P, Nosek J, Hofr C, Griffith JD,  
851 Tomaska L. 2016. Evolution of telomeres in *Schizosaccharomyces pombe* and its  
852 possible relationship to the diversification of telomere binding proteins. *PLoS One* **11**:  
853 e0154225.
- 854 Shakirov EV, Song X, Joseph JA, Shippen DE. 2009. POT1 proteins in green algae and land  
855 plants: DNA-binding properties and evidence of co-evolution with telomeric DNA.  
856 *Nucleic acids research* **37**: 7455-7467.
- 857 Shtessel L, Lowden MR, Cheng C, Simon M, Wang K, Ahmed S. 2013. *Caenorhabditis elegans*  
858 POT-1 and POT-2 repress telomere maintenance pathways. *G3: Genes| Genomes|*  
859 *Genetics* **3**: 305-313.
- 860 Sievers F, Higgins DG. 2021. The clustal omega multiple alignment package. In *Multiple*  
861 *sequence alignment*, pp. 3-16. Springer.
- 862 Simão FA, Waterhouse RM, Ioannidis P, Kriventseva EV, Zdobnov EM. 2015. BUSCO: assessing  
863 genome assembly and annotation completeness with single-copy orthologs.  
864 *Bioinformatics* **31**: 3210-3212.
- 865 Smythe AB, Holovachov O, Kocot KM. 2019. Improved phylogenomic sampling of free-living  
866 nematodes enhances resolution of higher-level nematode phylogeny. *BMC*  
867 *Evolutionary Biology* **19**: 1-15.
- 868 Sobinoff AP, Pickett HA. 2017. Alternative lengthening of telomeres: DNA repair pathways  
869 converge. *Trends in Genetics* **33**: 921-932.
- 870 Srinivasan J, Dillman AR, Macchietto MG, Heikkinen L, Lakso M, Fracchia KM, Antoshechkin I,  
871 Mortazavi A, Wong G, Sternberg PW. 2013. The draft genome and transcriptome of  
872 *Panagrellus redivivus* are shaped by the harsh demands of a free-living lifestyle.  
873 *Genetics* **193**: 1279-1295.
- 874 Stamatakis A. 2014. RAxML version 8: a tool for phylogenetic analysis and post-analysis of  
875 large phylogenies. *Bioinformatics* **30**: 1312-1313.
- 876 Stanke M, Diekhans M, Baertsch R, Haussler D. 2008. Using native and syntenically mapped  
877 cDNA alignments to improve de novo gene finding. *Bioinformatics* **24**: 637-644.
- 878 Stanke M, Schöffmann O, Morgenstern B, Waack S. 2006. Gene prediction in eukaryotes with  
879 a generalized hidden Markov model that uses hints from external sources. *BMC*  
880 *bioinformatics* **7**: 1-11.
- 881 Steinberg-Neifach O, Lue NF. 2015. Telomere DNA recognition in *Saccharomycotina* yeast:  
882 potential lessons for the co-evolution of ssDNA and dsDNA-binding proteins and  
883 their target sites. *Frontiers in Genetics* **6**: 162.
- 884 Sýkorová E, Fajkus J, Mezníková M, Lim KY, Neplechová K, Blattner FR, Chase MW, Leitch AR.  
885 2006. Minisatellite telomeres occur in the family Alliaceae but are lost in *Allium*.  
886 *American journal of botany* **93**: 814-823.



- 887 Sýkorová E, Lim K, Kunická Z, Chase M, Bennett M, Fajkus J, Leitch A. 2003. Telomere  
888 variability in the monocotyledonous plant order Asparagales. *Proceedings of the Royal*  
889 *Society of London Series B: Biological Sciences* **270**: 1893-1904.
- 890 Tomáška L, Nosek J, Sepšiová R, Červenák F, Juríková K, Procházková K, Neboháčová M,  
891 Willcox S, Griffith JD. 2019. Commentary: single-stranded telomere-binding protein  
892 employs a dual rheostat for binding affinity and specificity that drives function.  
893 *Frontiers in Genetics*: 742.
- 894 Tran TD, Cao HX, Jovtchev G, Neumann P, Novák P, Fojtová M, Vu GT, Macas J, Fajkus J,  
895 Schubert I. 2015. Centromere and telomere sequence alterations reflect the rapid  
896 genome evolution within the carnivorous plant genus *Genlisea*. *The Plant Journal* **84**:  
897 1087-1099.
- 898 Van Steensel B, Smogorzewska A, De Lange T. 1998. TRF2 protects human telomeres from  
899 end-to-end fusions. *Cell* **92**: 401-413.
- 900 Visacka K, Hofr C, Willcox S, Necasova I, Pavlouskova J, Sepsiova R, Wimmerova M,  
901 Simonicova L, Nosek J, Fajkus J. 2012. Synergism of the two Myb domains of Tay1  
902 protein results in high affinity binding to telomeres. *Journal of Biological Chemistry*  
903 **287**: 32206-32215.
- 904 Weiss H, Scherthan H. 2002. *Aloe* spp.–plants with vertebrate-like telomeric sequences.  
905 *Chromosome Research* **10**: 155-164.
- 906 Wong B. 2011. Color blindness. *nature methods* **8**: 441.
- 907 Yamamoto I, Zhang K, Zhang J, Vorontsov E, Shibuya H. 2021. Telomeric double-strand DNA-  
908 binding proteins DTN-1 and DTN-2 ensure germline immortality in *Caenorhabditis*  
909 *elegans*. *Elife* **10**: e64104.
- 910 Yoshimura J, Ichikawa K, Shoura MJ, Artiles KL, Gabdank I, Wahba L, Smith CL, Edgley ML,  
911 Rougvie AE, Fire AZ. 2019. Recompleting the *Caenorhabditis elegans* genome.  
912 *Genome research* **29**: 1009-1022.
- 913 Zhong Z, Shiue L, Kaplan S, de Lange T. 1992. A mammalian factor that binds telomeric  
914 TTAGGG repeats in vitro. *Molecular and cellular biology* **12**: 4834-4843.
- 915 Zhou Y, Wang Y, Xiong X, Appel AG, Zhang C, Wang X. 2022. Profiles of telomeric repeats in  
916 Insecta reveal diverse forms of telomeric motifs in Hymenoptera. *Life Science*  
917 *Alliance* **5**.

918

919



## Telomeric repeat evolution in the phylum Nematoda revealed by high-quality genome assemblies and subtelomere structures

Jiseon Lim, Wonjoo Kim, Jun Kim, et al.

*Genome Res.* published online November 2, 2023  
Access the most recent version at doi:[10.1101/gr.278124.123](https://doi.org/10.1101/gr.278124.123)

---

**Supplemental Material** <http://genome.cshlp.org/content/suppl/2023/11/21/gr.278124.123.DC1>

**P<P** Published online November 2, 2023 in advance of the print journal.

**Accepted Manuscript** Peer-reviewed and accepted for publication but not copyedited or typeset; accepted manuscript is likely to differ from the final, published version.

**Open Access** Freely available online through the *Genome Research* Open Access option.

**Creative Commons License** This manuscript is Open Access. This article, published in *Genome Research*, is available under a Creative Commons License (Attribution-NonCommercial 4.0 International license), as described at <http://creativecommons.org/licenses/by-nc/4.0/>.

**Email Alerting Service** Receive free email alerts when new articles cite this article - sign up in the box at the top right corner of the article or [click here](#).

---



---

To subscribe to *Genome Research* go to:  
<https://genome.cshlp.org/subscriptions>

---